Thermoelectric properties of nanostructured porous silicon

THERMOELECTRIC PROPERTIES OF NANOSTRUCTURED POROUS SILICON

R.J. Martín-Palma[1], H. Cabrera[2], B. Martín-Adrados[1], D. Korte[3], E. Pérez-Cappe[4], Y. Mosqueda[4], M.A. Frutis[5], and E. Danguillecourt[4,6]

[1] Departamento de Física Aplicada, Universidad Autónoma de Madrid, 28049 Cantoblanco, Madrid, Spain.

[2] The Abdus Salam International Centre for Theoretical Physics (ICTP), Strada Costiera 11,Trieste, Italy.

[3] Laboratory for Environmental and Life Sciences, University of Nova Gorica, Vipavska 13, Nova Gorica 5000, Slovenia.

[4] Institute of Materials Science and Technology (IMRE), Havana University, Zapata y G, Vedado, 10400 Havana, Cuba.

[5] Instituto Politécnico Nacional, Centro de Investigación en Ciencia Aplicada y Tecnología Avanzada, Unidad Legaria, Legaria 694, Col. Irrigación, Mexico City 11500, Mexico.

[6] Instituto Minero Metalurgico de Moa, Cuba.

ABSTRACT

In this work we report on the thermoelectric properties of nanostructured porous silicon (nanoPS) layers grown onto silicon substrates. More specifically, nanoPS layers of different porosity, nanocrystal size, and thickness were fabricated and their electrical conductivities, Seebeck coefficients, and thermal conductivities were subsequently measured. It was found that these parameters show a strong dependence on the characteristics of the nanoPS layers and thus can be controlled.

1. Introduction

Thermoelectric materials constitute a promising approach to provide a method for solid-state cooling and power generation without refrigeration or moving parts [1,2]. Consequently, different thermoelectric materials, such as Bi_2Te_3, PbTe, Cu_2S, Cu_2Se, skutterudites and clathrates [3-8], have been extensively studied. Despite that, the search for novel, high efficiency and low-cost materials is always open.

The overall performance of a thermoelectric system is given by the thermoelectric figure of merit, *ZT*, which character depends on the electrical conductivity, σ, Seebeck coefficient, *S*, absolute temperature, *T*, and the electrical and lattice contributions to the thermal conductivity, κ, i.e., $\kappa = \kappa_e + \kappa_l$ [1]:

$$ZT = \frac{\sigma S^2 T}{\kappa_e + \kappa_l} \quad (1)$$

Large values of *ZT* are associated to good thermoelectric performance. A high *ZT* requires high electrical conductivity and high Seebeck coefficient combined with low thermal conductivity. Good thermoelectrics are therefore crystalline materials that manage to scatter phonons without significantly disrupting the electrical conductivity. This behavior would require a rather unusual material, usually termed phonon-glass electron-crystal [9]. The phonon-glass requirement stems from the need for as low a lattice thermal conductivity as possible, which can potentially be achieved in some nanostructured complex materials [10].
Its low-cost and high-yield processing capabilities, make of Si the most-widely used material in the semiconductor industry. However, Si is considered a very inefficient thermoelectric material with *ZT* of the order of 0.01, although some theoretical works and experiments have demonstrated an increase in *ZT* for Si-based low-dimensional structures [11,12]. Moreover, by creating porous structures with pore sizes falling between the native electron and phonon mean free paths, it is possible to disturb phonon transport more than electron transport to increase the σ-to-κ ratio, and thus *ZT* [13].

Within this context, nanostructured porous silicon (nanoPS) has been identified as a material with a high potential to be used as a material for thermoelectric applications [14,15,16,17,18], based on the current tendency of using nanostructured bulk materials to improve the figure of merit of conventional materials. Nanostructured interfaces inside these materials strongly scatter phonons, but are expected to only slightly affect the charge carrier transport. As a result, such materials have shown significantly reduced lattice thermal conductivity, k_L, and in some cases simultaneously increased power factor $S^2\sigma$, resulting in *ZT* improvements over their bulk counterparts [19].

A great deal of interest was raised toward nanoPS when in 1990 strong visible photoluminescence at room temperature from p-type silicon wafers electrochemically etched in hydrofluoric acid (HF)-based solutions was reported [20]. As a result, since the beginning of the 1990s, nanoPS has stimulated much research and many potential applications in different fields have been pointed out. Indeed, several devices have been developed, including light-emitting diodes, optical filters [21], waveguides [22], photonic crystals, optical microcavities [23], capacitors, solar cells, biosensors and chemical sensors, and dielectric mirrors. Moreover, as a consequence of its particular properties, nanoPS has found increasing applications beyond traditional uses in the field of photonics to the field of biomedicine [24,25].

In this work, the thermoelectric properties of nanostructured porous silicon layers grown onto silicon substrates were determined. In particular, the dependence on porosity and thickness of the electrical resistivity, temperature dependence of the Seebeck coefficient, and the thermal conductivity was studied.

2. Experimental

2.1. Fabrication of the samples

Nanostructured porous silicon (nanoPS) layers were formed by the electrochemical etch, under different conditions, of boron-doped (p type) silicon wafers of <100> orientation and with a resistivity of 0.1–0.5 Ω·cm. The wafers were cut into 1.5×1.5 cm^2 pieces which were mounted into a sample holder with an exposed area to the electrochemical etching solution of 1 cm^2, which is the area where the thermoelectrical measurements are carried out. The electrolyte consisted of a 2:1 HF (48 wt %):ethanol (98 wt %) mixture. The wafers were etched galvanostatically under illumination from a 100 W halogen lamp for different times under current densities of 50, 100, and 150 mA/cm^2. The samples were immersed in ethanol after the formation of the nanoPS layers.

2.2. Current-voltage measurements

Ramp current-voltage (*I-V*) measurements were carried out using a Keithley 2611A sourcemeter unit. For this purpose, a ramp rate of 0.5 V/s was applied to the etched region of the silicon substrate. The thickness of the etched region was previously estimated in a Dektak^3 surface profile system.

The Seebeck coefficients were determined with a homemade apparatus, in which two Pt electrodes were attached to both sides of the sample to ensure efficient thermal and electrical contacts. Measurements were carried out in the 473 K to 673K temperature range in air at appropriate and fixed temperature gradients between the cold and warm poles. The temperature gradient was established with a microfurnace placed close to one of the platinum poles (warm pole). The voltage and temperature were monitored with accuracies of 0.1 mV and 0.1 K, respectively, as the system reaches the equilibrium. Both the voltage and temperature differences were recorded only when the variation of these parameters was less than ± 0.1 (mV, K), respectively. The system was calibrated with the aid of p and n standard semiconductors. The following equation was used to calculate the Seebeck coefficient:

$$S = -\frac{\Delta V}{\Delta T} \qquad (2)$$

2.3. Thermal conductivity measurements

The thermal conductivities of the different samples [26,27] were determined by means of photothermal beam deflection spectroscopy (BDS) [28-30]. The experimental setup is schematically shown in Figure 1. Light coming out from a He-Ne laser (excitation beam, EB) with a output wavelength of 632.8 nm and 35 mW output power (MELLES GRIOT, Model 25-LHP-928-230) is modulated by a mechanical chopper (SCIENTIC INSTRUMENTS, Control unit model 300C, chopping head model 300CD, chopping disks model 300H) and heats the sample. Since the examined sample is opaque, it is assumed that the whole incident light energy is absorbed by its surface. Due to radiationless processes, the absorbed energy is converted into heat inducing temperature oscillations (TOs) in the sample and fluid above it, that in turn causes a corresponding change in the index of refraction, and its gradients [29].

These variations are probed by a 543.5 nm output wavelength and 2 mW output power He-Ne laser (MELLES GRIOT, Model 25-LGR-393-230) called the probe beam (PB). PB travels through the region of temperature oscillations, parallel to the surface of the sample (transverse BDS in its skimming configuration), and as a result of what it is deflected. The amplitude and phase of the probe beam deflection is determined by the use of position sensor which is a quadrant photodiode (RBM - R. Braumann GmbH, Model C30846E) equipped with an interference filter (540 nm, MELLES GRIOT, model FL543.5-1) that filters PB before it enters the position sensor. The amplitude and phase of the BDS signal are measured by a lock-in amplifier (STANFORD RESEARCH INSTRUMENTS, model SR830 DSP) connected to a PC for data storage and processing. The examined sample is placed on a 3D translation stage (CVI, Model 2480M and 2488) to vary its position in the *x*, *y*, and *z* directions and optimize the experimental configuration. The measurements were performed in air at room temperature. PB is focused by a 25 mm diameter lens of 25 mm focal distance (EDMUND OPTICS) to have its waist of 50 μm radius over the sample, whereas EB is directed perpendicular to the surface of the sample by a broad band, flat mirror (400-750 nm, THORLABS, model BB1-E02) and shaped by a 25 mm diameter lens of 100 mm focal distance (EDMUND OPTICS) to form a spot of around 2 mm diameter onto the sample's surface.

For each sample, the amplitude and phase of the BDS was measured as a function of the modulation frequency of EB. The thermal conductivitie of the whole sample κ_{eff} (porous layer and substrate), as well as of substrate without porous layer κ_s was determined by comparing the measured results with theoretical values by the use of the least square fitting procedure [31]. To ensure high accuracy of the thermal conductivity determination, the measurements were conducted under "thermally thick" conditions. This is achieved for thermal diffusion

length of TOs shorter than the thickness of the examined sample. Thus, the range of modulation frequency of the EB was chosen to be from 300 Hz to 3 kHz [32].

The thermal conductivity of just the porous layer, κ_{pl}, was calculated by determining the thermal conductivity of whole sample and substrate only by the use of equation [28]:

$$\kappa_{pl} = \frac{\kappa_{eff}\kappa_s d}{\kappa_s (d+L) - \kappa_s L} \quad (3)$$

d and L being the thickness of the porous layer and the substrate, respectivelly.

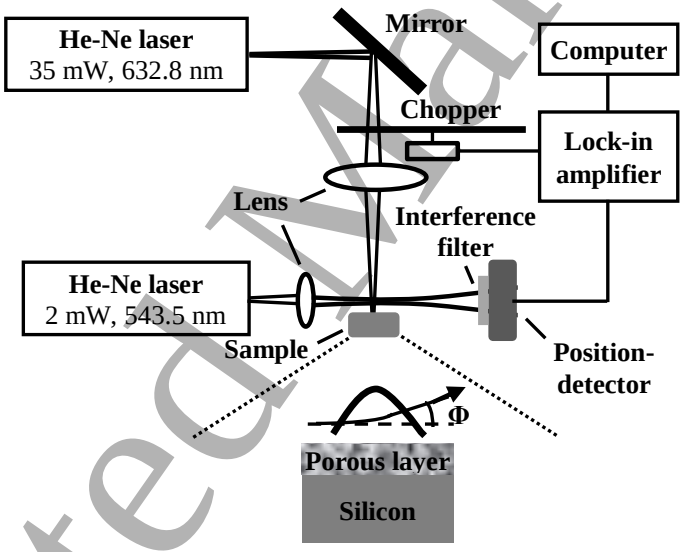

Figure 1. Experimental setup used for the BDS measurements. An excitation beam (EB) from continuous He-Ne laser (632.8 nm, 35 mW), modulated by a mechanical chopper illuminates the surface of the sample. The induced periodic variations in refractive index of air above the sample are sensed by the probe beam (PB) from a low power He-Ne laser (543.5 nm, 2 mW) and a position detector connected to the lock-in amplifier and PC.

3. Results and discussion

Figure 2 shows the typical morphology of nanostructured porous silicon (nanoPS) layers fabricated using three different current densities, namely 50, 100, and 150 mA/cm^2. Image

analysis allowed us to determine that increased fabrication current density results in higher porosity in addition to smaller nanocrysyal size.

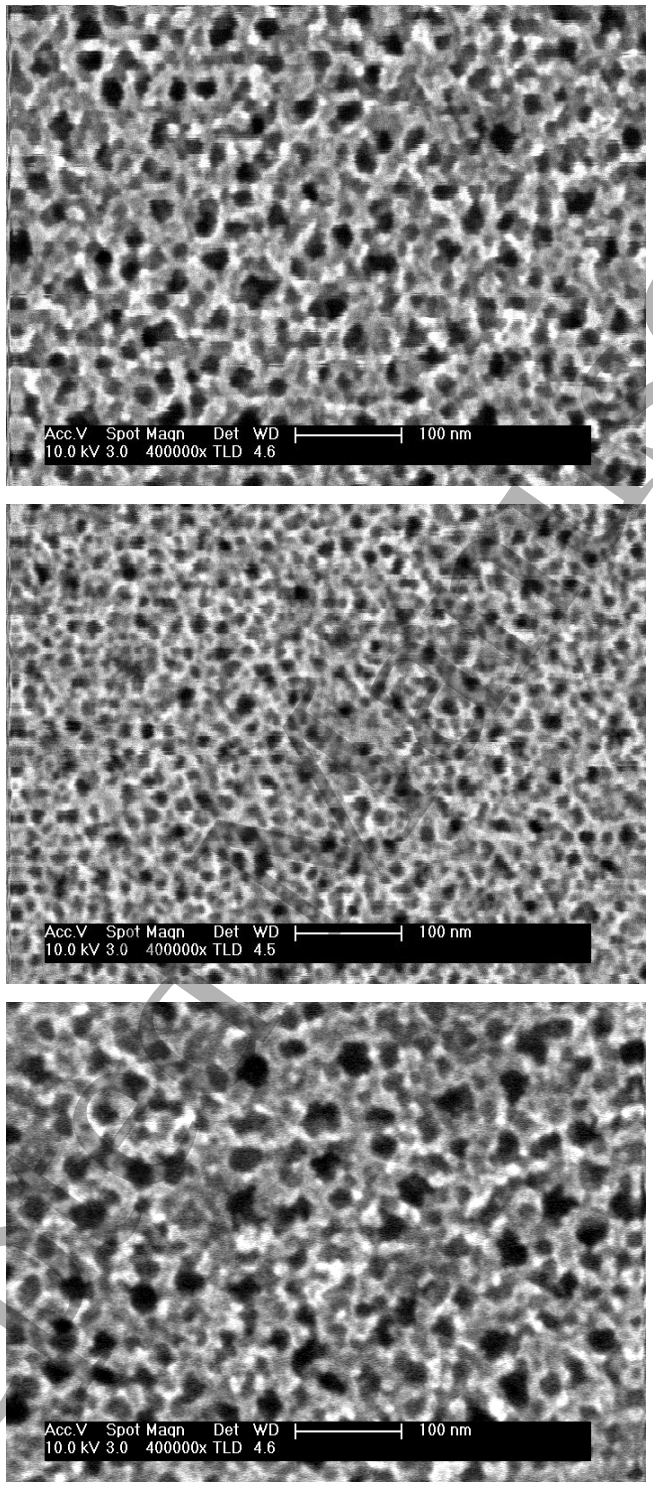

Figure 2. SEM top views of nanoPS layers fabricated using different current densities: (top) 50 mA/cm^2, (middle) 100 mA/cm^2, and (bottom) 150 mA/cm^2.

Additionally, Figure 3 shows a cross-sectional view of a typical nanoPS layer fabricated using a current density of 150 mA/cm^2. FESEM analysis allowed us to measure the thickness of the nanoPS layers, which are shown in Table 1.

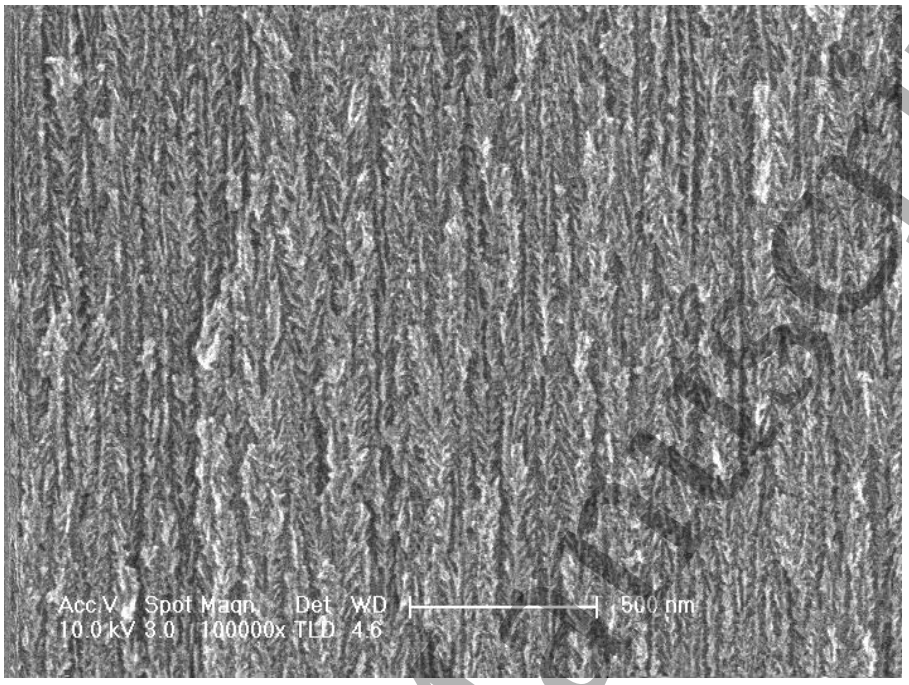

Figure 3. Cross-sectional view of a nanoPS layer fabricated under a current density of 150 mA/cm^2.

	Current density: 50 mA/cm^2	**Current density: 100 mA/cm^2**	**Current density: 150 mA/cm^2**
Anodization time (s)	**Thickness (microns)**		
200	10.8	17.5	24
600	32.5	52.5	72

Table 1. Summary of the thickness of the nanoPS layers prepared for this study.

The Figure 4 portrays the electrical conductivity variations of the nanoPS layers as a function of the fabrication current density to a fixed etching time (600 s). It is observed that the electrical conductivity enormously decreases with the fabrication current density, showing an exponential decay behavior. In general terms, it can be affirmed that the conductivity of the nanoPS layers decreases with (i) increasing fabrication current density (i.e., increasing porosity) and (ii) increasing etching time (i.e., increasing thickness of the nanoPS layer). The

enormous reduction of electrical conductivity with increasing porosity can be attributed to depletion of carriers associated to the increased effective band gap of nanoPS [33], as well as to increased surface scattering of charge carriers given by both a reduction of the nanocrystal size and an increased polycrystalline behavior for higher fabrication current density [34]. Besides, increased etching time results in thicker nanoPS layers which results in larger resistivity.

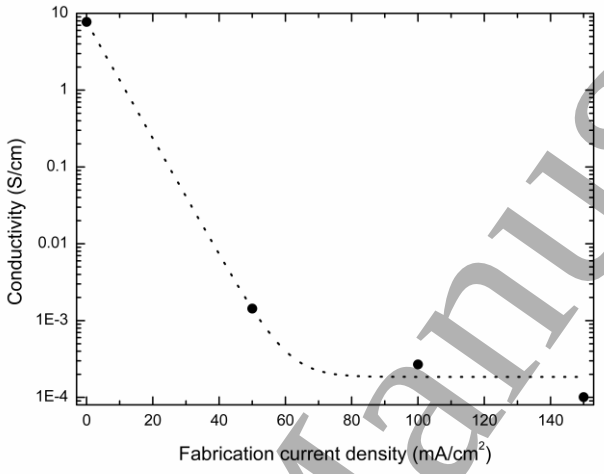

Figure 4. Electrical conductivity as a function of the fabrication current density and at etching time 600s.

The temperature dependence of the Seebeck coefficient for nanoPS layers with different characteristics was determined following the procedure described in Section 2.2. The experimental results are shown in Figures 5 and 6. The experimental results show that, independently of the thickness of the nanoPS layer (related to the etching time), the Seebeck coefficient increases with temperature. However, this behavior is the opposite in the case of highly-porous nanoPS layers (fabrication current density of 150 mA/cm^2), i.e., the Seebeck coefficient decreases for increasing temperature. The negative sign of the slope of the Seebeck coefficient indicates that, in this particular case, electrical conduction mainly occurs through electrons in the conduction band [35]. As such, increased porosity and smaller nanocrystal size results in a change of the character of the initial Si substrate (p type). As such, while holes are required for the fabrication of nanostructured porous silicon, the concentration of holes is reduced during the fabrication process.

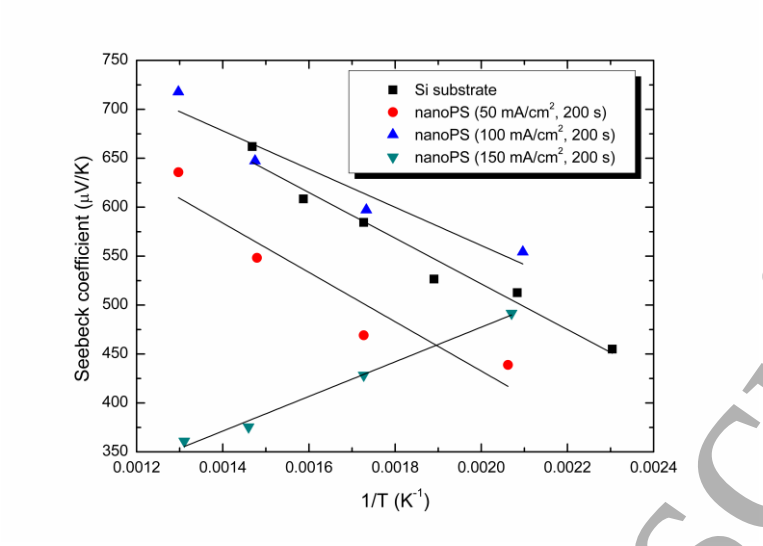

Figure 5. Temperature dependence of the Seebeck coefficient of the Si substrate and nanoPS layers fabricated under different current densities (50, 100, and 150 mA/cm^2). The etching time was 200 s.

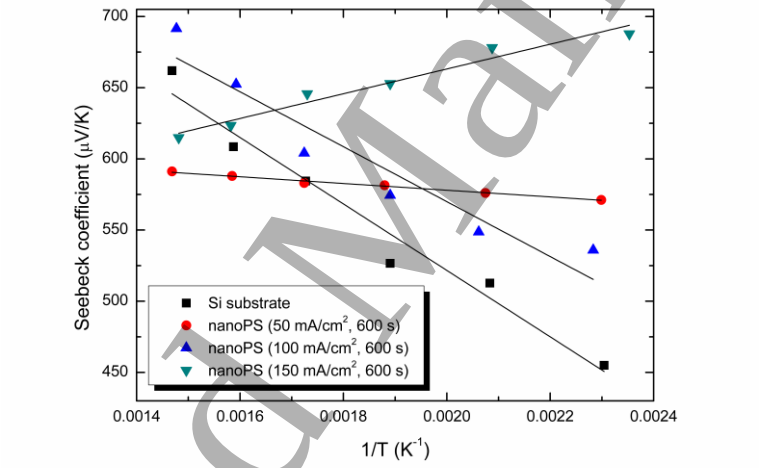

Figure 6. Temperature dependence of the Seebeck coefficient of the Si substrate and nanoPS layers fabricated under different current densities (50, 100, and 150 mA/cm^2). The etching time was 600 s. The connecting lines are just a guide to the eye.

The enhanced Seebeck coefficient of the nanoPS layers compared to that of the Si substrate can be considered an additional evidence of carrier depletion resulting from increased bandgap, possibly combined with energy-filtering effects [36]. In addition, phonon drag, i.e., reduction of carrier mobility as a consequence of increased effective mass of charge carriers, might contribute to an increment of the Seebeck coefficient. In all, the values of the Seebeck

coefficient can be considered to arise from an interplay between a reduction in charge-carrier diffusion with *T*, phonon drag, and boundary scattering.

In semiconductors, the variation of the Seebeck coefficient with the inverse of temperature takes the form [35]

$$S = \frac{k}{e}\left(\frac{E_s}{kT} + A\right) \quad (4)$$

E_s being the activation energy and A the heat of transport (considered temperature-independent), which represents the contribution to the Seebeck coefficient of electrons in states above the conduction band edge. As shown in Figures 5 and 6, the best fits are obtained for nanoPS layers fabricated under current densities of 150 mA/cm^2 in which, as previously discussed, electrons in the conduction band are mostly responsible of the electrical conduction. In the case of a fabrication time of 200 s, A = 1.43 and E_s = 0.177 eV. For a fabrication time of 600 s, A = 5.37 and E_s = 0.102 eV. For lower current densities, and thus lower porosity and larger nanocrystal size, the experimental results suggest that both the values of A and those of the activation energy are larger (A estimated between 7 and 11 and E_s up to 0.252 eV). Accordingly, the thermal conduction properties of nanoPS, as well as its electrical properties, can be controlled with two key parameters: fabrication current density and time, i.e., porosity/nanocrystal size, and thickness.

Regarding the values of *S* for a given temperature, previous works [18] have reported that by increasing porosity, the Seebeck coefficient increases and reaches a maximum for a given porosity. When the porosity is further increased, *S* decreases. A similar behavior has been observed in this work. This behavior may be related to the fact that in the case of highly porous materials the electrical conduction hindering process rises as a consequence of the presence of an increased amount of nanocrystals, grain boundaries, as well as silicon dioxide (SiO_2) and possibly suboxides. These compounds possess much lower electrical conductivity than Si. Altogether, this makes the material much more resistive when porosity is increased. Overall, this provokes a larger voltage drop and consequently an increase in the value of the Seebeck coefficient, an effect which is observed independently of the etching time (in our case, 200 s and 600 s). However, as discussed above, the character of the electrical conduction changes for nanoPS layers of very large porosity.

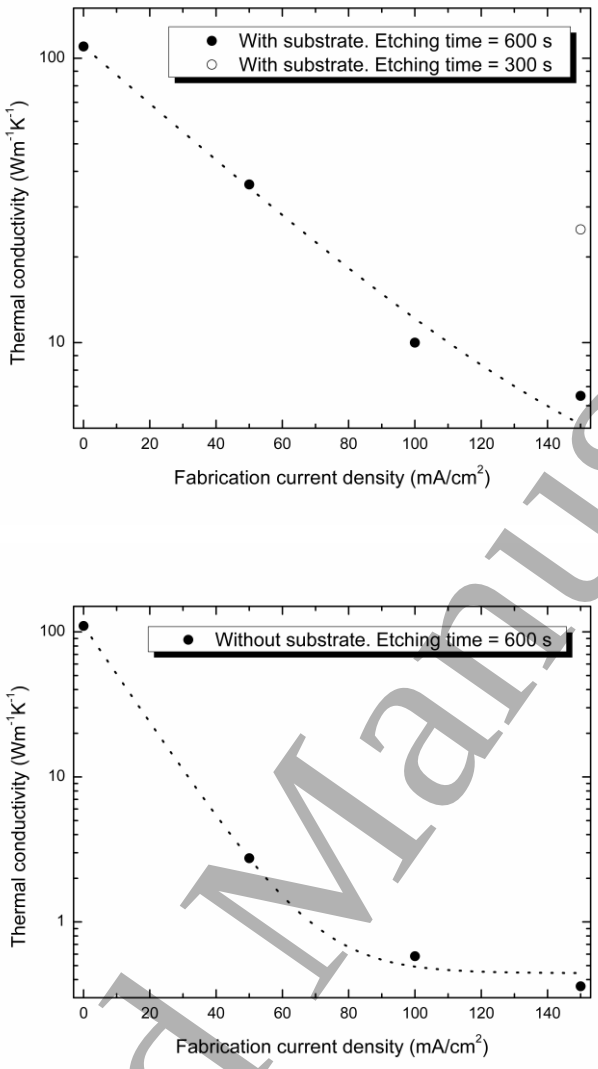

Figure 7. Thermal conductivity as a function of the fabrication current density (50, 100, and 150 mA/cm^2). The etching time was 600 s. (top) values including the Si substrate. (bottom) Without the substrate. One of the samples was fabricated with the following conditions: 150 mA/cm^2 and 300 s to determine the effect of the thickness.

Finally, the thermal conductivity measurements of the nanoPS layers, with and without considering the Si substrate, were carried out. From Figure 7 it is observed that, as expected, the thermal conductivity diminishes for increasing fabrication current density, i.e., increasing porosity. In both cases (with and without the Si substrate), the experimental results can be fitted to an exponential decay. Since increased fabrication current density, in addition to higher porosity, also results in smaller nanocrystal size, interface scattering of phonons will

increase, thus reducing thermal conductivity. In effect, as the size a given nanostructure becomes comparable to the mean free path, phonons collide with the nanocrysyal boundaries more often than in bulk materials [37]. Increased collisions result in increased resistance to heat flow, thus resulting in reduced effective thermal conduction. Also, when heat flows between the interfaces of the different constituents of nanoPS (mainly Si, SiO_2, and void space), a temperature drop is likely to develop as a consequence of the mismatch in the phonon velocity and density of these constituents. This phenomenon is usually termed thermal boundary resistance. This effect becomes more significant for increased boundaries, i.e., for increasing fabrication current density that results in increased porosity and reduced nanocrystal size.

Moreover, it is observed that for a given porosity, the thermal conductivity increases for decreasing nanoPS layer thickness. Accordingly, as in the previously studied physical parameters, porosity is a key factor in the control of the thermoelectric behavior of nanoPS layers. In addition, thermal conductivity has been determined to be larger when the Si substrate is considered, since heat generated in the nanoPS layers is eventually carried away by phonons in the substrate.

4. Conclusions

The thermoelectric properties of nanostructured porous silicon (nanoPS) layers of different characteristics grown onto silicon substrates were determined. In particular, the dependence on porosity and thickness of the electrical resistivity, temperature dependence of the Seebeck coefficient, and the thermal conductivity were studied. It was found that porosity and layer thickness, which can be controlled during the fabrication of nanoPS layers, are key parameters for the control of their thermoelectric behavior.

Additionally, the electrical conductivity of the nanoPS layers enormously decreases with increasing fabrication current density (i.e., increasing porosity and smaller nanocrystal size), showing an exponential decay behavior. This magnitude also decreases with increasing etching time (i.e., increasing thickness).

The Seebeck coefficient (S) increases and reaches a maximum for a given porosity. When the porosity is further increased, S decreases. Moreover, the Seebeck coefficient increases with

temperature. However, this behavior is the opposite for highly-porous nanoPS layers. This behavior indicates that, in this case, electrical conduction mainly occurs through electrons in the conduction band. Consequently, increased porosity and smaller nanocrystal size results in a change of the character of the initial Si substrate (from p type to n type). In all, the increased magnitude of *S* in nanoPS layers can be considered an interplay between different effects, namely a reduction in charge-carrier diffusion with temperature, phonon drag, and boundary scattering.

Finally, the thermal conductivity has been found to diminish with fabrication current density, i.e., with increased porosity and reduced nanocrystal size. Additionally, it was observed that for a given porosity, the thermal conductivity increases for decreasing nanoPS layer thickness.

DEDICATION

Dedicated to the memory of Arturo Jiménez Periáñez.

ACKNOWLEDGMENTS

R.J.M-P is grateful for funding provided by Ministerio de Economía y Competitividad (Spain), under project reference number MAT2014-54826-C2-1-R. H.C. would like to express gratitude to ICTP for support of this work through the Research Associateship and TRIL Programs. D.K. and M. F. would like to thank to CEEPUS CZ 2012 for support and thus enabling to perform the joint research, as well as to the Slovenian Research Agency for funding this work through research grants P1-0034: "Analytics and chemical characterization of materials and processes."

REFERENCES

1. D.M. Rowe, CRC Handbook of Thermoelectrics, CRC Press, Boca Raton, 1995.
2. DiSalvo FJ. Science 1999; 285:703–6.
3. A.I. Hochbaum, R. Chen, R.D. Delgado, W. Liang, E.C. Garnett, M. Najaria, A. Majumdarand, P. Yang, Nature 451 (2008) 163-167.
4. K. Biswas, J. He, I.D. Blum, C. Wu, T.P. Hogan, D.N. Seidman, V.P. Dravid, M.G. Kanatzidis, Nature 489 (2012) 414e418.
5. B.C. Sales, D. Mandrus, R.K. Williams, Science 272 (1996) 1325e1328. Y. Pei, H. Wang, G.J. Snyder, Adv. Mater. 24 (2012) 6125e6135.
6. Y. He, T. Day, T.S. Zhang, H.L. Liu, X. Shi, L.D. Chen, G.J. Snyder, Adv. Mater. 26 (2014) 3974e3978.
7. D.R. Brown, T. Day, K.A. Borup, S. Christensen, B.B. Iversen, G.J. Snyder, Apl. Mat. 1 (2013) 52107.
8. H. Kleinke, Chem. Mater. 22 (2010) 604-611.
9. Slack, G. A. in *CRC Handbook of Thermoelectrics* (ed. Rowe, M.) 407–440 (CRC, Boca Raton, 1995).
10. G. Jeffrey Snyder and Eric S. Tobere, Nature Materials 7, 105 - 114 (2008)
11. J.-H. Lee, G.A. Galli, and J.C. Grossman, Nanoporous Si as an Efficient Thermoelectric Material, NanoLetters 8(11), 3750-3754 (2008).
12. H. Lee, D. Vashaee, D.Z. Wang, M.S. Dresselhaus, Z. F. Ren, and G. Chen, Effects of nanoscale porosity on thermoelectric properties of SiGe, J. Appl. Phys 107, 094308 (2010).
13. D.W. Song *et al.*, APL 84(11), 1883 (2004).
14. J. Tang, H.-T. Wang, D. H. Lee, M. Fardy, Z. Huo, T. P. Russell, and P. Yang, Holey Silicon as an Efficient Thermoelectric Material, Nano Letters 10, 4279-4283 (2010).
15. J. de Boor, D.S. Kim, X. Ao, M. Becker,·N.F. Hinsche, I. Mertig, P. Zahn, and V. Schmidt, Thermoelectric properties of porous silicon, Applied Physics A (2012).
16. K Valalaki and A G Nassiopoulou, Low thermal conductivity porous Si at cryogenic temperatures for cooling applications, J. Phys. D: Appl. Phys. 46 (2013) 295101 (9pp).
17. H. Li, Y. Yu, and G. Li, Computational modeling and analysis of thermoelectric properties of nanoporous silicon, Journal of Applied Physics 115, 124316 (2014).

18. K. Valalaki, P. Benech, and A.G. Nassiopoulou, High Seebeck Coefficient of Porous Silicon: Study of the Porosity Dependence, Nanoscale Research Letters 11, 201 (2016).
19. Q. Hao *et al.*, APL 97, 063109 (2010)
20. L.T. Canham, Silicon quantum wire array fabrication by electrochemical and chemical dissolution of wafers, Appl Phys Lett57, 1046-8 (1990).
21. Frohnhoff S, Berger MG. Porous silicon superlattices. Adv Mater 1994;6:963-5
22. Loni A, Canham LT, Berger M, et al. Porous silicon multilayer optical waveguides. Thin Solid Films 1996;276:143-6
23. Pellegrini V, Tredicucci A, Mazzoleni C, et al. Enhanced optical properties in porous silicon microcavities. Phys Rev B 1995;52:R14328-31
24. R.J. Martín-Palma, M. Manso-Silván, and V. Torres-Costa, Biomedical applications of nanostructured porous silicon: a review, Journal of Nanophotonics 4, 042502 (2010).
25. J. Hernández-Montelongo, A. Muñoz-Noval, J.P. García-Ruíz, V. Torres-Costa, R.J. Martín-Palma, and M. Manso-Silván, Nanostructured porous silicon: the winding road from photonics to cell scaffolds – a review, Frontiers in Bioengineering and Biotechnology 3, 60 (2015).
26. M. Pawlak, M. Chirtoc, N. Horny, J. Pelzl, J Appl Phys 119, 125108 – 125108 (2016).
27. M. Pawlak, A. Panas, A. Ludwig, A. D. Wieck, Thermochim. Acta 650, 33 – 38, (2017).
28. D. Trefon-Radziejewska, J. Bodzenta, Optical Materials **45**, 2015, DOI: 10.1016/j.optmat.2015.03.007.
29. J. Bodzenta, A. Kazmierczak-Bałata, R. Bukowski, M. Nowak, B. Solecka, Int. J. Thermophys. **38(6)**, 93, 2017.
30. A. Kazmierczak-Bałata, J. Mazur, J. Bodzenta, D. Trefon-Radziejewska, L. Drewniak, Int. J. Thermophys. **35(12)**, 46, 2014).
31. Korte, D., Franko, M., 2015. Application of complex geometrical optics to determination of thermal, transport, and optical parameters of thin films by the photothermal beam deflection technique. Journal of the Optical Society of America A. 32, 61-74.
32. Korte, D., Cabrera, H., Toro, J., Grima, P., Leal, C., Villabona, A., and Franko, M.. Optimized frequency dependent photothermal beam deflection spectroscopy. *Laser physics letters*, 2016, vol. 13, no. 12, pp. 1-12.
33. R.J. Martín-Palma, J. Pérez-Rigueiro and J.M. Martínez-Duart, Study of carrier transport in metal/porous silicon/Si structures. Journal of Applied Physics 86(12), 6911 (1999).

34. R. J. Martín-Palma, L. Pascual, P. Herrero, and J.M. Martínez-Duart, Direct determination of grain sizes, lattice parameters, and mismatch of porous silicon, Appl. Phys. Lett. 81(1), 25 (2002).
35. R.G. Mathur, R.M. Mehra, and P.C: Mathus, J. Appl. Phys. 83(11), 5855 (1998).
36. D. Narducci, E. Selezneva, G. Cerofolini, S. Frabboni, and G. Ottaviani, Impact of energy filtering and carrier localization on the thermoelectric properties of granular semiconductors, Journal of Solid State Chenistry 193 (2012) 19-25.
37. G. Chen, Phonon heat conduction in nanostructures, Int. J. Therm. Sci. 39, 471-480 (2000).